THE JOURNAL OF PHYSICAL CHEMISTRY C
A JOURNAL OF THE AMERICAN CHEMICAL SOCIETY

pubs.acs.org/JPCC

Article

Photoelectrochemical Properties of BODIPY-Sensitized Anodic TiO_2 Layers Decorated with AuNPs for Enhanced Solar Performance

Karolina Syrek,* Joanna Czopor, Monika Topa-Skwarczyńska, Maciej Pilch, Kamil Kamiński, Joanna Ortyl,* and Grzegorz D. Sulka

Cite This: *J. Phys. Chem. C* 2023, 127, 9471−9480

Read Online

ACCESS | Metrics & More | Article Recommendations | Supporting Information

ABSTRACT: An efficient hybrid photoanode based on the anodic TiO_2 layer covered with gold nanoparticles (AuNPs) and BODIPY (boradiazaindacene) microrods for solar-driven water splitting experiments was developed. The BODIPY derivative (B-1) was synthesized, and their stability in different solvents was characterized in order to prepare the heterojunction photoelectrode. An insight into materials' properties was gained by evaluating their morphology, optical, semiconducting, and photoelectrochemical performance. By combining the unique morphology of anodic TiO_2 nanotubes with the electron trapping abilities of AuNPs and the light absorption properties of the BODIPY dye, a novel heterojunction photoanode generating 15 times higher photocurrent (~120 μA cm^{-2}) than pristine anodic TiO_2 (~8 μA cm^{-2}) was obtained.

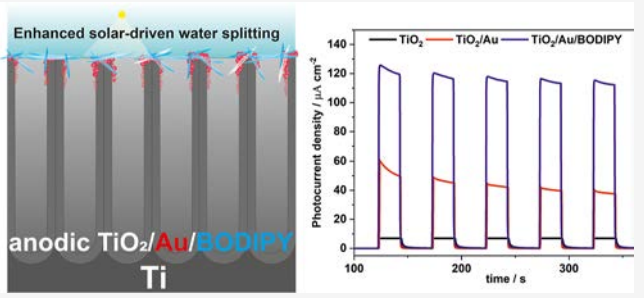

1. INTRODUCTION

Given their unique geometry, anodic TiO_2 nanotubes show extraordinary chemical, electrical, photocatalytic, and optical properties that make them considered for a variety of applications, for example, dye-sensitized solar cells (DSSCs),[1,2] photocatalysis,[3,4] photoelectrochemistry,[5,6] gas sensors,[7] batteries,[8] biomaterials,[9] and more. Considering the limitations of its effective use in visible light, the engineering of new hybrid materials based on coupling with co-catalyst,[10] doping,[11] defects engineering,[12] and sensitization[13,14] (with other semiconductors, polymers,[15,16] or dyes) is still broadly exploited. Sensitization of TiO_2 with dyes is often used for creating solar cell systems. To date, anodic TiO_2 was coupled with a commonly studied Ru(II) complex dye (N719),[2,17−22] P3DT [poly (3-decylthiophene)],[22] and boradiazaindacenes known as BODIPY dyes[23] as donors for heterojunction solar cells.

BODIPY dyes are a very attractive group of compounds with useful fluorescent labels for biomolecules,[24] and their new derivatives have found applications as chemosensors,[25] light absorbers,[26] logic gates,[27] theranostic agents for photodynamic therapy,[28] and photoinitiators for cationic photopolymerization for 3D printing.[29,30] One of the advantages of BODIPY dye sensitization for energy-related applications[31−33] (DSSC or photocatalytic) compared to commercial N719 is a metal-free structure, which makes it more cost-effective and environmentally friendly.[34] What is more, the B−N bond offers good dye stability in different solvents.[35]

There are very few reports on coupling the BODIPY dye with TiO_2.[23] For instance, Jayworth et al.[36] studied the covalent attachment of BODIPY and dipyrrin molecules to the surface of TiO_2 nanoparticles. In the case of metal oxides, such bonding typically requires the presence of an anchoring group (e.g., a carboxylic acid group). It was shown that even without the introduction of anchors in the BODIPY structure, the unmodified dye can bind to the TiO_2 surface via its BF_2 group through boron−oxygen surface bonds, as long as the 3 and 5 positions of the pyrrole rings are unsubstituted. It was also reported that BODIPY-based dyes are characterized by ultrafast electron injection into the conduction band of TiO_2 nanoparticles, indicating that the electron injection is not inhibited by any binding-induced structural changes.[36]

Another interesting study devoted to nanotubular TiO_2 sensitized with the BODIPY dyes was reported by Gonzalez-Valls et al.[23] It was shown that DSSCs with BODIPY dye molecules have 27 times higher incident photon-to-current efficiency (IPCE) than with a commercially available N719 dye. It was demonstrated that the amount of B3 BODIPY adsorbed on the TiO_2 NTs surface was 100 times smaller than the commercial N719 dye. This indicates a strong absorption

Received: February 10, 2023
Revised: April 26, 2023
Published: May 15, 2023

coefficient of the B3 dye, efficient photon-to-electron conversion, and BODIPY dye injection efficiency, which was especially evidenced for IPCE normalized to the quantity of the dye for each solar cell. These results clearly showed the great potential of BODIPY molecules as sensitizers.

To the best of our knowledge, BODIPY dye-sensitized TiO_2 layers were only considered until now as electrodes in DSSC cells. Here, we present for the first time novel photoanodes based on anodic TiO_2 layers covered with gold nanoparticles (AuNPs) and BODIPY microrods for solar-driven water splitting experiments. The BODIPY derivative was synthesized, and its stability in different solvents was characterized to produce the efficient photoelectrode. The material properties were comprehensively elucidated by studying their morphology, composition, optical, semiconducting, and photoelectrochemical performance.

2. EXPERIMENTAL SECTION

2.1. Synthesis of BODIPY B-1. All inorganic salts, organic reagents, and solvents were analytically pure and used without further purification. The chromophore 4,4-difluoro-1,3,5,7,8-pentamethyl-4-bora-3a, 4a-diaza-*s*-indacene (BODIPY B-1) was used in this research. The compound has previously been used as a precursor/intermediate for the preparation of iodonium salts to initiate cationic and radical photopolymerization processes.[30] The synthesis procedure of the chromophore consisted of 3 steps. In the first step, 2,4-dimethylpyrrole (21 mmol) was dissolved in dichloromethane (DCM, 8 cm^3), purged with argon, and then acetyl chloride (49 mmol) was added dropwise to the mixture for 30 min. Subsequently, 40 cm^3 hexane was added, after which the mixture was evaporated to dryness. In the next step, the residue was dissolved in 97 cm^3 DCM, then triethylamine (61 mmol) was added to the mixture, and the whole mixture was stirred for 10 min under argon at room temperature. After that, in the 3rd step, 262 mmol boron trifluoride diethyl ether was added to the mixture, and the overall mixture was continuously stirred for 1 h under argon at room temperature. The progress of the reaction was verified using thin-layer chromatography (TLC). After completion of the reaction, the mixture was washed with a saturated aqueous $NaHCO_3$ solution and dried over Na_2SO_4, then the solvents were evaporated, and the compound was purified using ethyl acetate crystallization. The structure and purity of the obtained products were confirmed by NMR and LC−MS analysis. The reaction scheme is shown in Figure 1, and synthesis details as well as ^1H and ^{13}CNMR spectra were presented in our previous article.[30]

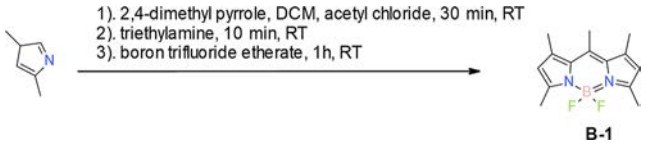

Figure 1. Scheme for the synthesis of the chromophore 4,4-difluoro-1,3,5,7,8-pentamethyl-4-bora-3a, 4a-diaza-*s*-indacene (BODIPY B-1).

2.2. Synthesis of Anodic TiO_2 Layers. The Ti foil (99.5% purity, 0.25 mm thick) was degreased in acetone and ethanol and subjected to electrochemical and chemical polishing according to the procedure previously reported.[37] The anodic titanium dioxide layers were prepared by a three-step anodization process in ethylene glycol containing NH_4F (0.38 wt %) and H_2O (1.79 wt %) at a constant potential of 40 V. The process was performed at 20 °C in a two-electrode cell, where the Ti sample was used as an anode and the Ti plate as a cathode. The first and second anodizing steps were carried out for 3 h. The oxide films formed during the first and second steps of anodization were removed using an adhesive tape. Before the third anodization, the electrochemical cell was filled with a fresh portion of the electrolyte, and the sample was anodized for 10 min. Afterward, the sample was annealed in air at 400 °C (with a heating rate of 2 °C min^{-1}) for 2 h using a muffle furnace (model FCF 5SHM Z, Czylok, Poland).

2.3. Photodeposition of AuNPs and Deposition of BODIPY Microrods on the TiO_2 Surface. AuNPs were synthesized by photoreduction of $HAuCl_4$ in the presence of anodic TiO_2 and UV light.[38] A mixture used for the photoreduction process consisted of 0.24 M $HAuCl_4$ and 0.3 M citric acid solutions mixed in a 1:39 volume ratio. The annealed TiO_2 sample was immersed in 2.5 mL of the as-prepared mixture and was irradiated in a photoreactor (Instytut Fotonowy, Poland) with UVA lamps for 15 min. The absorbance of the solution before and after the synthesis was measured using the Lambda 750S spectrometer (PerkinElmer) in the range of 250−800 nm. The AuNPs diameter and their zeta potential in the solution after photoreduction were measured using the Malvern Zetasizer Nano ZS. In the next step, 50 mg of BODIPY (B-1) dye was dissolved in 5 mL of acetone, and 2 μL of the solution was drop-cast on the surface of annealed TiO_2 (1 cm^2) and then dried in air for 24 h.

2.4. Characterization Methods. Fluorescence emission spectra of synthesized BODIPY B-1 in various solvents with different polarities were recorded using a HORIBA spectrofluorometer at varied excitation and observation wavelengths in the range of 200−800 nm. The emission spectrum was collected in the range of 480−680 nm. The excitation wavelength was 365 nm, and the spectral bandwidth was set at 0.6 nm. 3D emission spectra were also recorded with the spectrofluorometer FluoroMAX 4Plus with the MicroMax Plus microwell plate reader (HORIBA, Kyoto, Japan), which was used for standard 96-well plates (Thermo Scientific). The scanning range of 3D fluorescence was 300−800 nm, in which the excitation wavelength started at 300 nm and ended at 600 nm with a step of 2 nm and an emission bandwidth of 0.6 nm.

The morphology of prepared electrodes was examined using field-emission scanning electron microscopy (FE-SEM/EDS, Hitachi S-4700). Fourier-transform infrared spectroscopy (FTIR) spectra were recorded using a Nicolet iS10 FT-IR spectrometer with an attenuated total reflectance (ATR) attachment (SMART iTX) (Waltham, MA, USA). AuNPs were centrifuged at 10,000 rpm for 10 min and then dried under a reduced pressure at 40 °C. Fluorescence microscopy imaging was performed using a Nikon Eclipse LV100 microscope in fluorescence mode with a Prior Lumen 200 light source. The UV−vis diffuse reflectance spectra (UV−Vis DRS) were recorded using the LAMBDA 750S spectrometer (PerkinElmer) equipped with an integrating sphere module in the range of 250−800 nm.

2.5. Electrochemical and Photoelectrochemical Tests. Electrochemical measurements were carried out in a Teflon cell with a quartz window in a three-electrode system, where anodic TiO_2 layers were used as the working electrode (WE), a platinum foil as the counter electrode (CE), and a saturated calomel electrode (SCE) as the reference electrode (RE). The

https://doi.org/10.1021/acs.jpcc.3c00931
J. Phys. Chem. C 2023, 127, 9471−9480

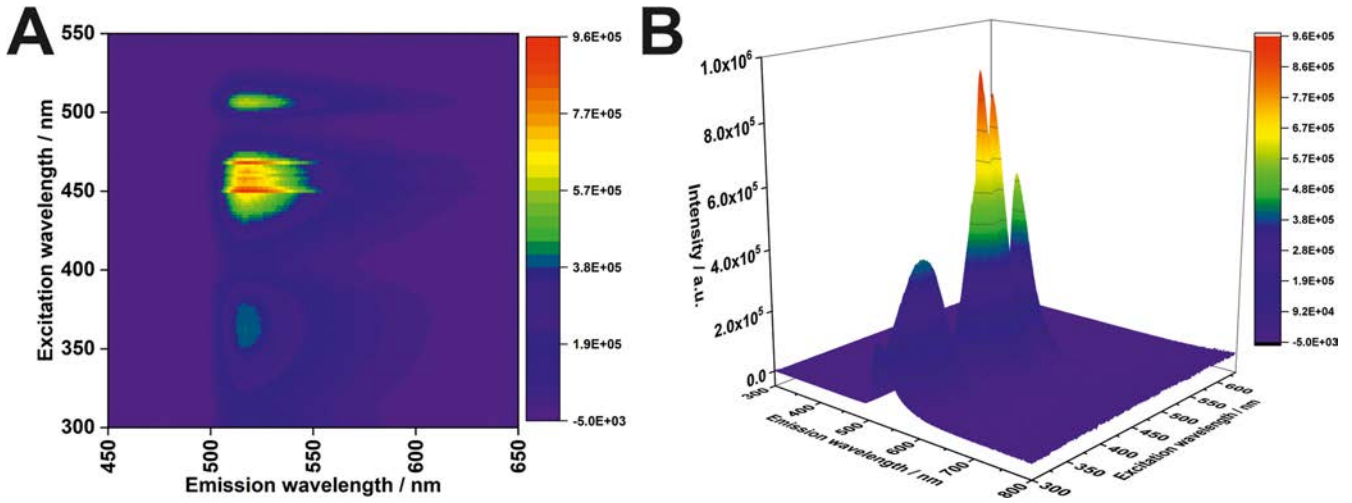

Figure 2. 4,4-Difluoro-1,3,5,7,8-pentamethyl-4-bora-3a, 4a-diaza-*s*-indacene (BODIPY B-1) spectrum in acetonitrile in 2D (A) and 3D (B) projections.

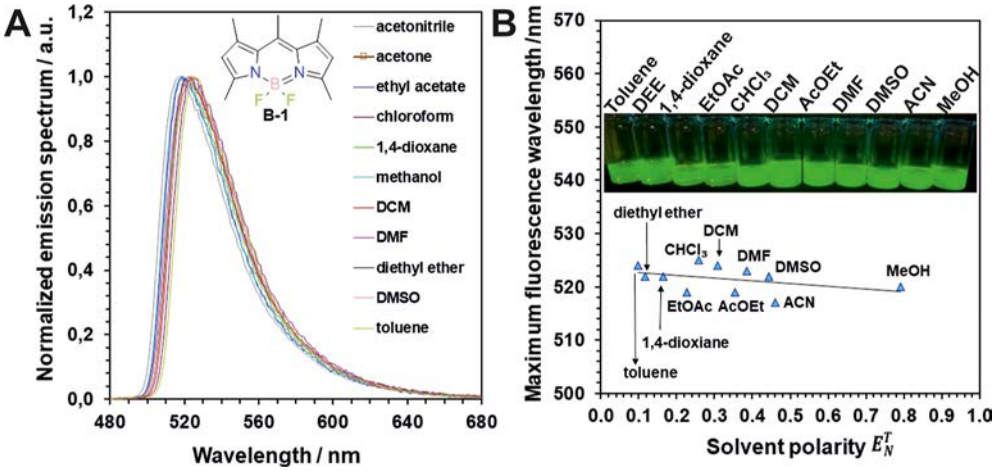

Figure 3. (A) Normalized fluorescence emission spectra for 4,4-difluoro-1,3,5,7,8-pentametylo-4-bora-3a,4a-diaza-*s*-indacene (BODIPY B-1) in solvents with different polarities. (B) Position of the emission intensity peak as a function of the normalized solvent polarity E_N^T for BODIPY B-1. Inset: pictures of fluorescence vials filled with BODIPY B-1 in various solvents.

WE was illuminated with AM 1.5 G standard sunlight using a xenon illuminator of 150 W (Instytut Fotonowy, Poland) combined with the PalmSens4 (PalmSens BV, The Netherlands) potentiostat. The generated photocurrents were measured in 0.1 M KNO_3 (pH = 6) and with the addition of 10% vol ethanol.

The semiconducting properties of the studied materials were studied using a Mott−Schottky analysis performed in a three-electrode system using the Gamry Reference 3000 potentiostat. Measurements were carried out in the dark at frequencies of 200, 500, and 1000 Hz during the cathodic scan.

3. RESULTS AND DISCUSSION

3.1. BODIPY Solvatochromic Effect. BODIPY dyes are unique fluorophores that can be used in many fields due to their remarkable photophysical properties, such as high molar absorption, tunable absorption and emission energies, and high fluorescence quantum yield.[30] The synthesized BODIPY derivative B-1 exhibits absorption up to 500 nm and emission up to 640 nm in acetonitrile (Figure 2).

In order to support the reproducibility and stability of the proposed TiO_2/Au/BODIPY photoelectrodes, BODIPY B-1 stability tests were performed in different solvents, and the solvatochromic effect was studied. The solvatochromic effect results from a change in the energy of a molecule in a solution relative to the energy of a free molecule. The energy of the free molecule consists of, among others, dispersion interactions—mainly the polarization of the molecule, electrostatic interactions, and the solvent Stark effect. The Stark effect occurs when there is a fluctuation of the solvent in the vicinity of a non-polar solute molecule, which in turn leads to the electric field weakening. For this goal, the BODIPY chromophore was dissolved in solvents having different polarities, such as acetonitrile, acetone, ethyl acetate, chloroform, 1,4-dioxane, methanol, DCM, dimethylformamide, diethyl ether, dimethyl sulfoxide, and toluene. The effect of solvent polarity on the emission spectra of the BODIPY chromophore was studied using the normalized solvent polarity E_N^T scale. This scale assumes that tetramethylsilane (TMS) is the least polar solvent and has the E_N^T value of 0, while water is the most polar solvent and has the E_N^T value of 1. The value of E_N^T for a given solvent can be calculated from the following eq 1[39,40]

https://doi.org/10.1021/acs.jpcc.3c00931
J. Phys. Chem. C 2023, 127, 9471−9480

$$E_N^T = \frac{E_T(\text{solvent}) - E_T(\text{TMS})}{E_T(\text{water}) - E_T(\text{TMS})} = \frac{E_T(\text{solvent}) - 30.7}{32.4} \quad (1)$$

where E_T is solvent polarity.

No significant changes in the emission spectrum of the studied BODIPY chromophore were observed when solvents with different polarities were used (Figure 3). This shows that the BODIPY B-1 dye is extremely stable in solvents with different polarities, which is extremely important for its further applications (Table 1S, Supporting Information). In addition, a correlation between solvent polarity expressed in the E_N^T scale and fluorescence emission intensity was also performed, from which it is obvious that solvent polarity does not affect considerably the emission spectrum of BODIPY B-1 (Figure 3B). Based on these data, we decided to use acetone as a solvent to prepare a BODIPY solution for further studies.

3.2. Preparation of Anodic TiO_2/Au/BODIPY Materials. The schematic diagram of the fabrication process of anodic TiO_2/Au/BODIPY electrodes is presented in Figure 4.

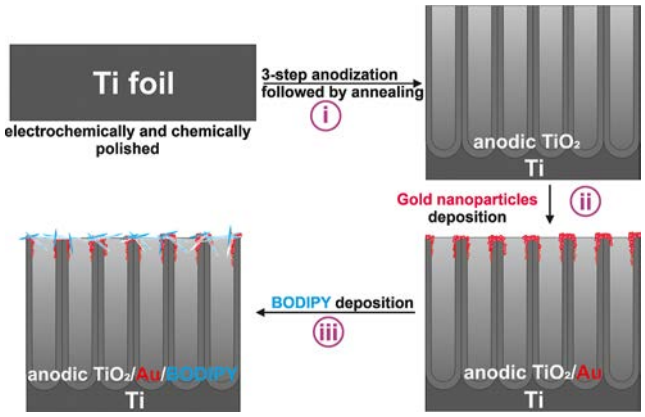

Figure 4. Schematic diagram of the fabrication process of (i) anodic TiO_2 nanotubes, (ii) anodic TiO_2/Au, and (iii) anodic TiO_2/Au/BODIPY.

It is widely recognized that a multi-step anodizing procedure of some metals, for example, Al[41,42] and Ti,[41,43] results in highly ordered porous/tubular oxide structures, which have a crucial impact on photoelectrochemical applications.[44] It was reported that the chemically and electrochemically polished Ti surface facilitates the formation of TiO_2 layers with highly ordered pore/tube arrangements.[37] Therefore, the polished titanium surface was subjected to a 3-step anodization process at constant voltage, and then synthesized layers were annealed at 400 °C to obtain the anatase TiO_2 phase (Figure 4, stage i).[6,45] In the second step, annealed TiO_2 layers were used as a catalyst and substrate for the deposition of Au nanoparticles by the photoreduction of $HAuCl_4$ in the presence of UV light (Figure S1A, Supporting Information). As a result, AuNPs were synthesized on the surface of the nanotubular TiO_2 substrate (Figure 4, stage ii). In the final step, the BODIPY B-1 dye was drop-cast on Au/TiO_2 materials to form the final electrode (Figure 4, stage iii). The morphology of the obtained materials at each preparation stage is presented in Figure 5.

The characteristic morphology of TiO_2 with an ordered arrangement of nanotubes having a regular inner tube diameter of ∼55 nm is presented in Figure 5A. As can be seen, after the photodeposition, the surface of the semiconducting material was evenly covered with AuNPs with a diameter of 20−30 nm (Figure 5B). The hydrodynamic diameter of AuNPs estimated in the remaining solution just after photodeposition (Figure S1B, Supporting Information) was around 10 nm, which suggests that during the drying of the electrode material, nanoparticles agglomerate on its surface. The morphology of the fabricated hybrid electrode (anodic TiO_2/Au/BODIPY) is presented in Figure 5C,D (with the corresponding EDS mapping, Figure 5E,F). The BODIPY B-1 microrods are dispersed uniformly over the whole TiO_2 surface and have a diameter of 0.4−1.5 μm and a length of 1−90 μm. The energy-dispersive X-ray spectroscopy (EDS) mapping confirmed the presence of Ti, O, C, F, and Au. It is also clearly visible that microrods are mainly composed of carbon and some traces of fluoride, for which EDS maps evidently overlap with the SEM image of the spindle BODIPY microrod (Figure 5D). Moreover, the distribution of AuNPs over the material surface is uniform, as confirmed by the EDS elemental mapping presented in Figure 5E.

The chemical composition of the studied materials was also confirmed by FTIR analysis (Figure 6A). A bare substrate (TiO_2 nanotubes) does not show any visible oscillations, while, after the deposition of AuNPs, peaks from Au (highlighted in beige) appeared at ∼1400 and ∼1700 cm^{-1}. These data are consistent with those reported in the literature.[46] For TiO_2/BODIPY, the appearance of dye is indicated by two peaks at ∼1200 and ∼1550 cm^{-1} (highlighted in yellow).[47,48] In the final material (TiO_2/Au/BODIPY), all the above-mentioned oscillations are present, suggesting a successful surface loading of both AuNPs and dye on TiO_2 nanotubes. Moreover, to confirm that the BODIPY dye preserved its fluorescence properties after deposition on the TiO_2/Au material, a confocal image was taken (Figure 6B). The fluorescence emitted by the specimen was clearly detected. One of the key parameters influencing the semiconducting properties of the materials is their ability to absorb the radiation, which is expressed by the band gap energy. The DRS UV−Vis spectra of the studied materials (Figure 6C) show characteristic reflectance minima at around 350 nm, which are related to the band gap energy in the TiO_2 anatase structure. Enhanced absorption in the region of 450−800 nm (compared to anodic TiO_2 layers) was observed for the samples with deposited AuNPs, and the presence of BODIPY microrods raised it even further. Enhanced absorption of TiO_2/Au materials at around 500−550 nm is caused by localized surface plasmon resonance (LSPR),[49] in which peak position and intensity depend on the nanoparticle size and shape. Another important factor which can potentially change the electronic structure of anodic TiO_2 is the strong metal−support interaction (SMSI), which is an interaction between the AuNPs and the surface of anodic TiO_2.[49−51] It can result in the generation of local point defects such as Ti^{3+} sites and oxygen vacancies in the oxide lattice,[52,53] which in turn can enhance visible light absorption by TiO_2.[52] It is widely recognized that the presence of point defects in the semiconductor structure is responsible for the generation of mid gap states, which result in the modification of absorption/reflectance spectra. What is more, the deposition of dye on the TiO_2/Au substrate improved the absorption of the material, especially in the visible range (600−800 nm) as previously reported by Gee et al.[48] To calculate the optical band gap energy, the DRS spectra were transformed into the Kubelka−Munk function and then plotted as Tauc's relations (Figure 6D). It is widely recognized that anodic TiO_2 layers annealed at 400 °C for 2 h in the air have the anatase crystal structure[6]

https://doi.org/10.1021/acs.jpcc.3c00931
J. Phys. Chem. C 2023, 127, 9471−9480

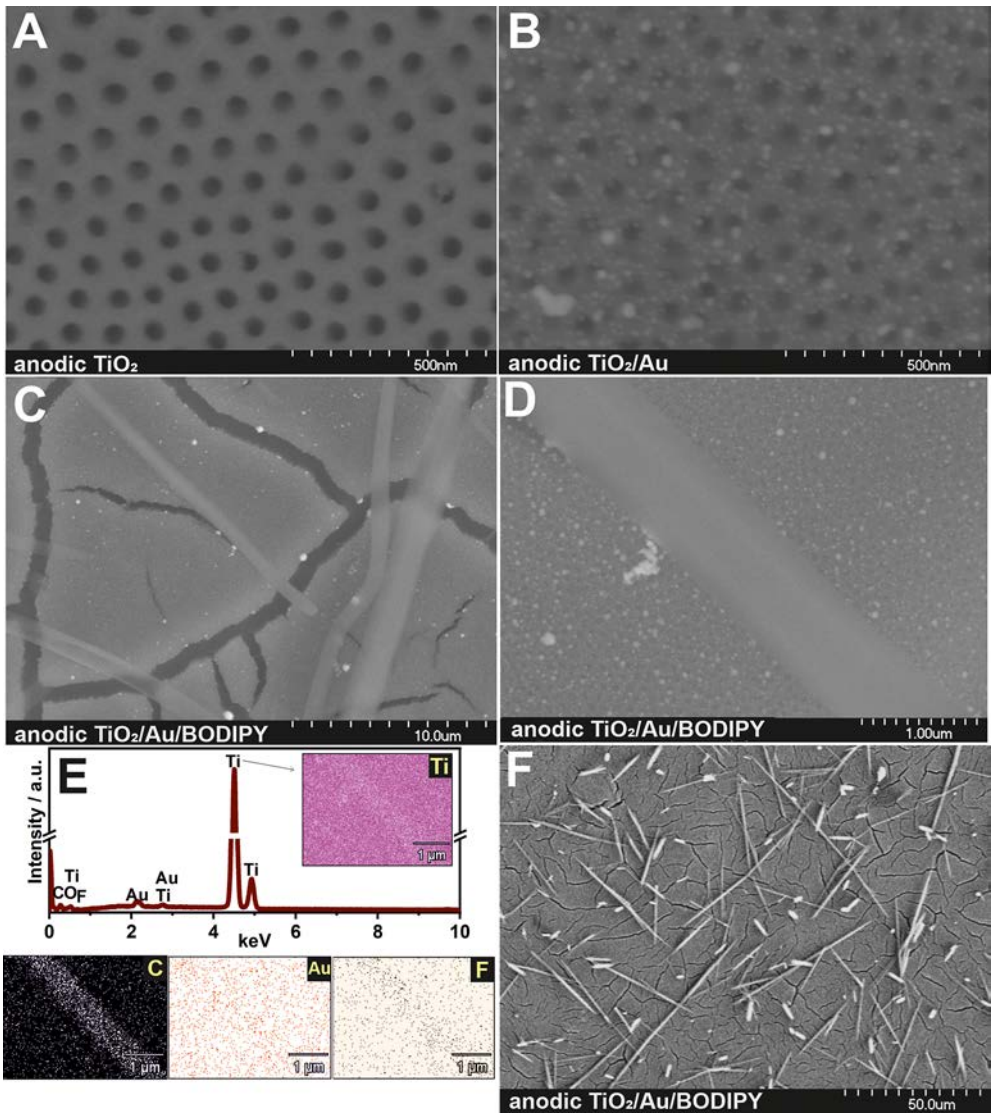

Figure 5. SEM images of anodic TiO_2 layers (A), anodic TiO_2 with deposited AuNPs (B), and anodic TiO_2 with deposited AuNPs and BODIPY B-1 microrods (C–F). Corresponding EDS analysis of the TiO_2/Au/BODIPY material (E).

with a characteristic band gap of 3.3 eV, and consequently, such a band gap is observed also for the studied TiO_2/Au and TiO_2/Au/BODIPY materials (Figure 6B). Moreover, for the modified materials, changes in the Tauc plots in the range of 2.6–2.0 eV are observed due to enhanced absorption caused by AuNPs. What is more, for the TiO_2/Au/BODIPY sample, another band gap with an energy of 1.8 eV is clearly visible and is related to the presence of the BODIPY dye, as previously reported.[23,32,54]

The studied materials were used as photoanodes for light-assisted water splitting (Figure 7) under monochromatic (Figure 7A) and solar (Figure 7B–D) illumination. Monochromatic light in the wavelength range of 300–450 nm was used for the illumination of photoanodes polarized at 1 V vs SCE in a 0.1 M KNO_3 solution (Figure 7A, inset). The obtained photocurrent densities were converted into IPCE values using the following eq 2[6,13]

$$\mathrm{IPCE} = 1240 \cdot \frac{I_p(\lambda)}{P(\lambda)\lambda'} \qquad (2)$$

where $I_p(\lambda)$ is the photocurrent density (A cm^{-2}) at the wavelength λ (nm), $P(\lambda)$ is the incident power density of light (W m^{-2}) at the wavelength λ (nm), and 1240 is a constant (W nm A^{-1}). It can be seen that anodic TiO_2 and TiO_2/Au are characterized by maximum IPCE at 350 nm; however, generated photocurrents at the AuNPs-modified TiO_2 photoanode are higher. Enhanced TiO_2/Au properties are connected to the excitation of Au LSPR that might promote photocatalytic reactions on the TiO_2 surface according to (i) hot electron transfer from Au LSPR to the TiO_2 conduction band, (ii) plasmonic-induced resonance energy transfer (PRET), or (iii) plasmon-induced local heating.[49,50] Moreover, the presence of AuNPs may improve the electron lifetime and reduce the rate of charge recombination.[55]

The additional deposition of BODIPY microrods on the TiO_2/Au surface affects the IPCE spectrum in the UV/violet spectral region and increases its intensity in visible light (up to c.a. 410 nm). This effect can be attributed to the enhanced absorption ability of the created heterojunction.[56] A second set of photoelectrochemical tests was carried out under simulated solar light at the same polarization conditions (Figure 7B). For

https://doi.org/10.1021/acs.jpcc.3c00931
J. Phys. Chem. C 2023, 127, 9471–9480

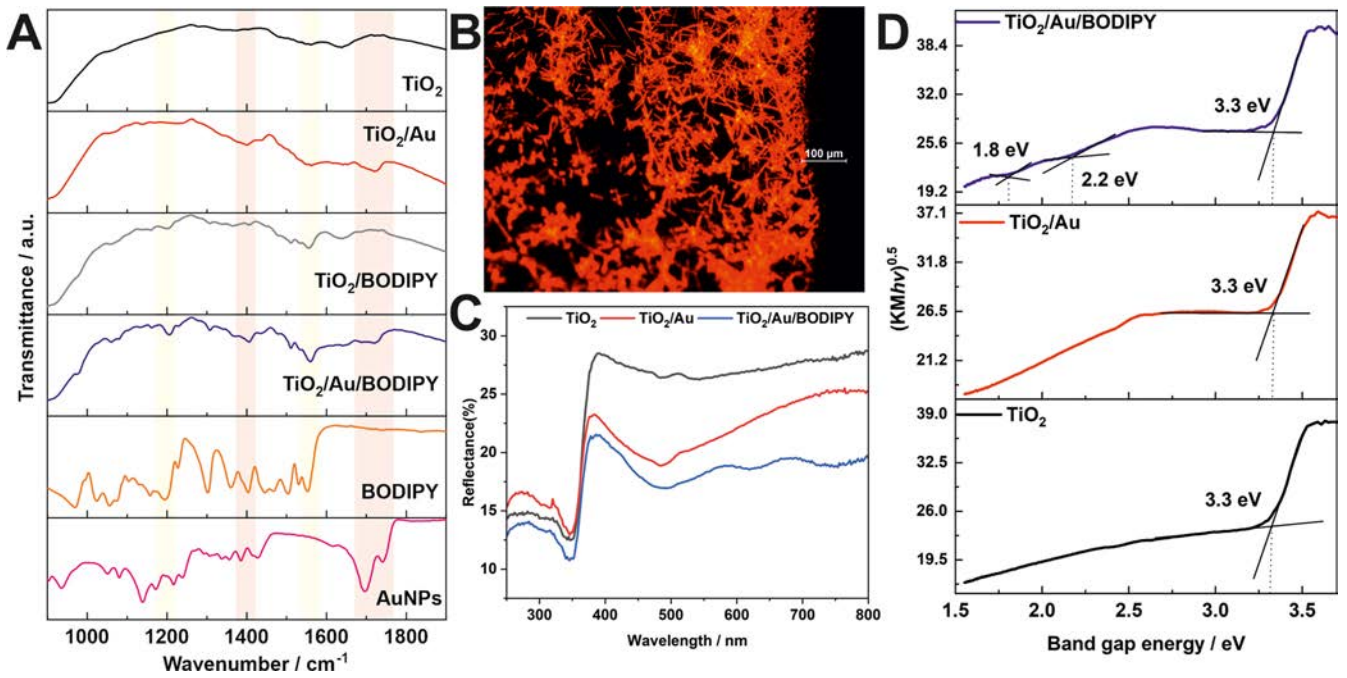

Figure 6. FTIR spectra recorded for studied materials (A). Confocal microscopy image of the TiO_2/Au/BODIPY electrode (B). DRS UV−Vis spectra of studied materials (C) with corresponding Tauc plots (D).

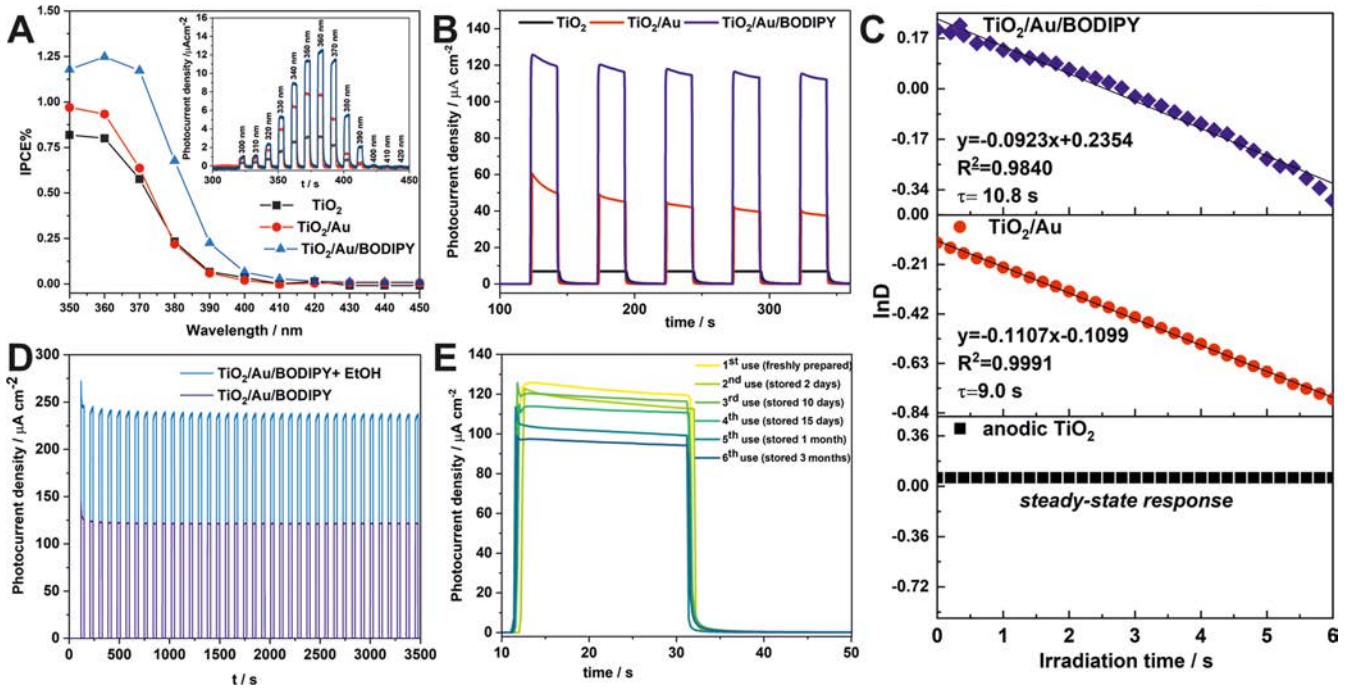

Figure 7. IPCE vs wavelength spectra calculated for tested photoanodes (inset: corresponding photocurrent density vs time curves measured at 1 V vs SCE during sequential illumination with the wavelength in the range of 300−450 nm) (A). Photocurrent density recorded in a 0.1 M KNO_3 solution at 1 V vs SCE during the chopped illumination with the solar simulator equipped with a 1.5 AirMass filter for all studied materials (B). ln *D* vs illumination time for all tested photoanodes (C). Photocurrent density recorded for TiO_2/Au/BODIPY in the presence of a 10 vol % hole scavenger (ethanol) (D). Photocurrent density generated over 3 months at the TiO_2/Au/BODIPY electrode during water splitting experiments (E).

simulated solar light illumination, the differences in the effectiveness of the tested electrodes are much more pronounced. Anodic TiO_2 generates a photocurrent density of about 8 μA cm^{-2}; however, after the deposition of AuNPs, a fourfold increase in photocurrent density can be seen. When the photoelectrode is additionally sensitized with the BODIPY B-1dye, the photoresponse is over 14 times higher. For the TiO_2/BODIPY electrode, a photocurrent density of ∼6 μA cm^{-2} is observed, which suggests a blocking effect of the dye on the activity of the TiO_2 electrode rather than enhancing its properties (Figure S2, Supporting Information). This clearly

https://doi.org/10.1021/acs.jpcc.3c00931
J. Phys. Chem. C 2023, 127, 9471−9480

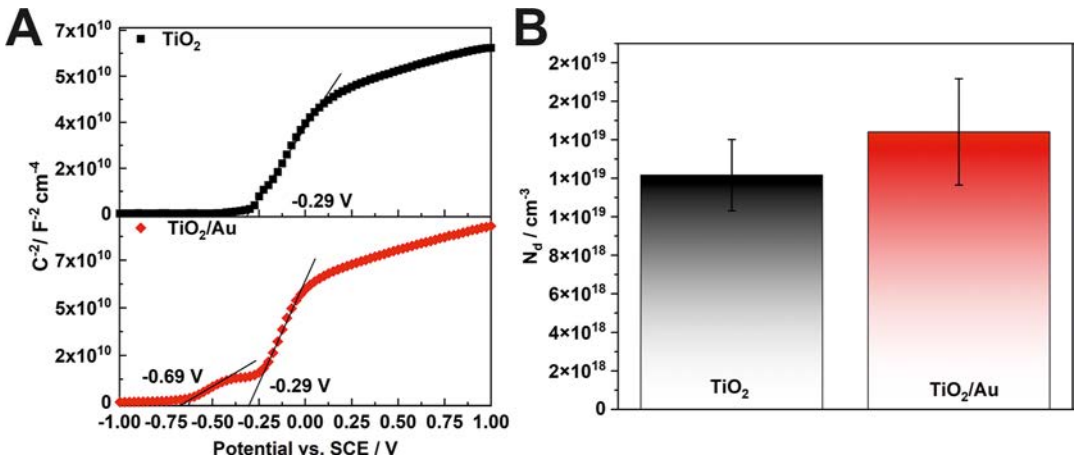

Figure 8. Mott−Schottky analysis performed for TiO_2 and TiO_2/Au electrodes at 1 kHz (A). Corresponding donor density averaged over different frequencies (B).

demonstrates that the presence of AuNPs is crucial to obtaining an effective heterostructured photoanode.

To gain a better understanding of the photoelectrochemical phenomena taking place during the exposure of photoanodes to solar illumination, the electron−hole recombination kinetics was calculated based on the following eq 3[57,58]

$$D = \left(\frac{J_t - J_{ss}}{J_0 - J_{ss}}\right) = e^{(-t/\tau)} \tag{3}$$

where J_0 is the photocurrent peak, J_{ss} is the steady-state photocurrent, J_t is the photocurrent at time t, and τ is the transient time constant. The higher the transient time constant, the slower the recombination of charge carriers. The recombination of photogenerated charge carriers may occur as a result of the accumulation of electrons in the semiconductor bulk and holes near its surface and/or the trapping of electrons or holes at surface states. To determine a recombination time constant, ln D vs time curves were plotted and are presented in Figure 7C. For the anodic TiO_2, a steady-state photocurrent was observed as a result of the applied potential of 1 V vs SCE. This result fits into the voltage-dependent charge recombination phenomenon of anodic TiO_2 reported in our previous paper.[59] Comparing the calculated transient time constants for the modified anodic TiO_2 photoanodes, it is visible that the presence of AuNPs on the nanostructured TiO_2 surface is not as effective the charge separation factor as the additional deposition of BODIPY B-1 microrods, which prolongs τ by an extra 1.8 s. These results clearly indicate that the organic component (BODIPY dye) of the hybrid photoanode slows down the electron−hole recombination process. To confirm this observation, a hole scavenger (ethanol) was added to the electrolyte, and the test was repeated (Figure 7D). The higher photoresponse of the TiO_2/Au/BODIPY electrode in the presence of ethanol can be attributed to the effective scavenging of holes by alcohol molecules, resulting in decreased recombination losses. What is more, this effect is also connected with the current doubling effect resulting from the direct oxidation of the ethanol radical at the material surface, which gives an additional free electron.[60,61]

Long-term stability tests were carried out over 3 months by measuring, at certain time intervals, the photocurrent generated at the TiO_2/Au/BODIPY photoanode in the photoelectrochemical water splitting experiments (Figure 7E). The results showed a 20% decrease in the photocurrent response after 3 months of storage at room conditions (Figure S3, Supporting Information). Nevertheless, the generated photocurrent was still much higher than for the unmodified TiO_2 and TiO_2/Au samples.

To understand better how the studied TiO_2/Au/BODIPY heterojunction works, the energy levels of the conduction and valence bands of the electrodes should be estimated. The flat band potential and donor densities were estimated at the frequencies of 200, 500, and 1000 Hz using Mott−Schottky analysis eq 4[62]

$$C_{SC}^{-2} = \left(\frac{2}{\varepsilon\varepsilon_0 q N_d}\right)\left(E - E_{fb} - \frac{kT}{q}\right) \tag{4}$$

where C_{sc} is the capacitance of the space charge region (F cm^{-2}), N_d is the donor density (cm^{-3}), ε is the dielectric constant of TiO_2 (100),[6] ε_0 is the permittivity of free space (8.85×10^{-14} F cm^{-1}), q is the electron charge (1.602×10^{-19} C), E is the applied potential (V), E_{fb} is a flat band potential (V), T is the absolute temperature (K), and k is the Boltzmann constant (1.38×10^{-23} J K^{-1}). A linear dependence of C_{sc}^{-2} vs applied potential with a positive slope (Figure 8A) indicates n-type semiconducting behavior. As can be seen, anodic TiO_2 is an n-type semiconductor with a flat band potential of −0.29 V vs SCE, which in fact represents the interfacial capacitance of the electric double layer at the semiconductor-/electrolyte interface. After the deposition of AuNPs on the TiO_2 surface, a second more negative flat band energy can be observed, and it is related to the formation of the Schottky barrier at the semiconductor-/metal interface. These observations are consistent with literature reports.[63] Moreover, the donor densities were estimated for both photoelectrodes (Figure 8B), and an increase in the donor density from 1.2×10^{-19} cm^{-3} for TiO_2 to 1.5×10^{-19} cm^{-3} for TiO_2/Au was observed (for details, see Table S2, Supporting Information).

Figure 9 presents an energy diagram for the TiO_2/Au/BODIPY heterojunction photoanode exposed to solar irradiation. The incident photon causes excitation of the BODIPY dye molecule. The highest occupied molecular orbital (HOMO) primarily consists of π-electron framework of BODIPY and styryl groups, with a significant contribution from π electrons of the diphenylamino substituent, while the

https://doi.org/10.1021/acs.jpcc.3c00931
J. Phys. Chem. C 2023, 127, 9471−9480

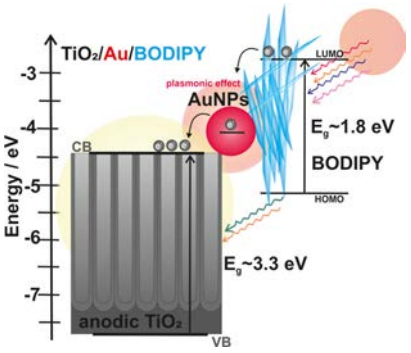

Figure 9. TiO_2/Au/BODIPY heterojunction photoanode while exposed to solar irradiation.

lowest unoccupied molecular orbital (LUMO) is typically formed from π electrons of the anchor group.[24] The reported energies of the LUMO (−3.31 eV) and HOMO (−5.05 eV) were used for the construction of our energy diagram.[23] The electrons from the excited BODIPY B-1 dye are transferred to the AuNPs, in which the plasmonic effect of gathering the electrons helps for the delocalization of the photogenerated electrons and, consequently, increases the efficiency of the electron−hole pair separation. Then, the electrons that have a higher energy than the Schottky barrier can be injected into the conduction band of the semiconductor. Moreover, direct tunneling of some electrons from the dye to the semiconductor, AuNPs, should be also considered.[64,65]

4. CONCLUSIONS

By combining the unique morphology of anodic TiO_2 nanotubes with the electron trapping abilities of AuNPs and the light absorption properties of the BODIPY dye, a novel efficient hybrid photoanode for photoelectrochemical water splitting was developed. The BODIPY dye microrods had a diameter of 0.43−1.5 μm and a length ranging from 1 to 90 μm. BODIPY microrods were uniformly deposited over the TiO_2 surface with dispersed Au nanoparticles.

The obtained TiO_2/Au/BODIPY electrode generated over 14 times higher photocurrent than pristine anodic TiO_2. The calculated transient time constants indicated that at the applied potential conditions, the presence of AuNPs on the surface of TiO_2 nanotubes increased the rate of charge carrier recombination, which was further inhibited by the additional deposition of BODIPY microrods. Moreover, the TiO_2/Au/BODIPY photoelectrode showed a satisfying photoresponse even after 3 months of storage, and after the storage period, the generated photocurrent was still over 10 times higher than that observed for pristine anodic TiO_2.

■ ASSOCIATED CONTENT

Supporting Information

The Supporting Information is available free of charge at https://pubs.acs.org/doi/10.1021/acs.jpcc.3c00931.

BODIPY solvatochromic effect; preparation of Au nanoparticles by photodeposition; photoelectrochemical properties of the TiO_2/BODIPY electrode; stability of the photoelectrochemical response of TiO_2/Au/BODIPY; and Mott−Schottky analysis—flat band potential (PDF)

■ AUTHOR INFORMATION

Corresponding Authors

Karolina Syrek − *Faculty of Chemistry, Department of Physical Chemistry and Electrochemistry, Jagiellonian University, 30-387 Krakow, Poland;* orcid.org/0000-0002-4041-9100; Phone: +48126862770; Email: syrek@chemia.uj.edu.pl, karolina.syrek@uj.edu.pl; Fax: +48126862750

Joanna Ortyl − *Department of Biotechnology and Physical Chemistry, Faculty of Chemical Engineering and Technology, Cracow University of Technology, 30-155 Krakow, Poland; Photo HiTech Ltd., 30-348 Krakow, Poland; Photo4Chem Ltd., 30-133 Krakow, Poland;* orcid.org/0000-0002-4789-7199; Email: joanna.ortyl@photohitech.com, jortyl@pk.edu.pl

Authors

Joanna Czopor − *Faculty of Chemistry, Department of Physical Chemistry and Electrochemistry, Jagiellonian University, 30-387 Krakow, Poland*

Monika Topa-Skwarczyńska − *Department of Biotechnology and Physical Chemistry, Faculty of Chemical Engineering and Technology, Cracow University of Technology, 30-155 Krakow, Poland;* orcid.org/0000-0002-3201-6379

Maciej Pilch − *Department of Biotechnology and Physical Chemistry, Faculty of Chemical Engineering and Technology, Cracow University of Technology, 30-155 Krakow, Poland;* orcid.org/0000-0002-7792-6587

Kamil Kamiński − *Faculty of Chemistry, Department of Physical Chemistry and Electrochemistry, Jagiellonian University, 30-387 Krakow, Poland;* orcid.org/0000-0002-7421-6758

Grzegorz D. Sulka − *Faculty of Chemistry, Department of Physical Chemistry and Electrochemistry, Jagiellonian University, 30-387 Krakow, Poland;* orcid.org/0000-0001-7431-617X

Complete contact information is available at: https://pubs.acs.org/10.1021/acs.jpcc.3c00931

Notes

The authors declare no competing financial interest.

■ ACKNOWLEDGMENTS

The SEM imaging was performed in the Laboratory of Field-Emission Scanning Electron Microscopy and Microanalysis at the Institute of Geological Sciences, Jagiellonian University, Poland. The BODIPY synthesis was funded by the MEiN from budget funds for science in the years 2018−2022, as a research project under the "Diamond Grant" program ("Synthesis and testing of application properties of new high-performance initiating photosystems dedicated to new generation photo-cured dental composites"; contract number 0052/DIA/2018/47).

■ REFERENCES

(1) Varghese, O. K.; Paulose, M.; Grimes, C. A. Long vertically aligned titania nanotubes on transparent conducting oxide for highly efficient solar cells. *Nat. Nanotechnol.* **2009**, *4*, 592−597.

(2) Jen, H. P.; Lin, M.-H.; Li, L.-L.; Wu, H.-P.; Huang, W. K.; Cheng, P.-J.; Diau, E. W.-G. High-performance large-scale flexible dye-sensitized solar cells based on anodic TiO_2 nanotube arrays. *ACS Appl. Mater. Interfaces* **2013**, *5*, 10098−10104.

(3) Wierzbicka, E.; Zhou, X.; Denisov, N.; Yoo, J.; Fehn, D.; Liu, N.; Meyer, K.; Schmuki, P. Self-enhancing H_2 evolution from TiO_2 nanostructures under illumination. *ChemSusChem* **2019**, *12*, 1900−1905.
(4) Lee, H.; Kumbhar, V. S.; Lee, J.; Oh, H.; Lee, K. Boosted photocatalytic hydrogen evolution by tuning inner pore size and co-catalyst thickness of the anodic TiO_2 nanotubes. *Catal. Today* **2021**, *359*, 3−8.
(5) Hou, X.; Fan, L.; Zhao, Y.; Lund, P. D.; Li, Y. Highly active titanium oxide photocathode for photoelectrochemical water reduction in alkaline solution. *J. Power Sources* **2022**, *524*, 231095.
(6) Syrek, K.; Sennik-Kubiec, A.; Rodriguez-Lopez, J.; Rutkowska, M.; Żmudzki, P.; Hnida-Gut, K. E.; Grudzień, J.; Chmielarz, L.; Sulka, G. D. Reactive and morphological trends on porous anodic TiO_2 substrates obtained at different annealing temperatures. *Int. J. Hydrogen Energy* **2020**, *45*, 4376−4389.
(7) Perillo, P. M.; Rodríguez, D. F. A room temperature chloroform sensor using TiO_2 nanotubes. *Sens. Actuators, B* **2014**, *193*, 263−266.
(8) Galstyan, V.; Macak, J. M.; Djenizian, T. Anodic TiO_2 nanotubes: A promising material for energy conversion and storage. *Appl. Mater. Today* **2022**, *29*, 101613.
(9) Pawlik, A.; Rehman, M. A. U.; Nawaz, Q.; Bastan, F. E.; Sulka, G. D.; Boccaccini, A. R. Fabrication and characterization of electrophoretically deposited chitosan-hydroxyapatite composite coatings on anodic titanium dioxide layers. *Electrochim. Acta* **2019**, *307*, 465−473.
(10) Wu, Z.; Hwang, I.; Cha, G.; Qin, S.; Tomanec, O.; Badura, Z.; Kment, S.; Zboril, R.; Schmuki, P. Optimized Pt single atom harvesting on TiO_2 nanotubes—Towards a most efficient photocatalyst. *Small* **2022**, *18*, 2104892.
(11) Chahrour, K. M.; Ooi, P. C.; Eid, A. M.; Nazeer, A. A.; Madkour, M.; Dee, C. F.; Wee, M. M. R.; Hamzah, A. A. Synergistic effect of bi-phased and self-doped Ti^{+3} on anodic TiO_2 nanotubes photoelectrode for photoelectrochemical sensing. *J. Alloys Compd.* **2022**, *900*, 163496.
(12) Zhou, X.; Liu, N.; Schmuki, P. Photocatalysis with TiO_2 Nanotubes: "Colorful" Reactivity and Designing Site-Specific Photocatalytic Centers into TiO_2 Nanotubes. *ACS Catal.* **2017**, *7*, 3210−3235.
(13) Sołtys-Mróz, M.; Syrek, K.; Wiercigroch, E.; Małek, K.; Rokosz, K.; Raaen, S.; Sulka, G. D. Enhanced visible light photoelectrochemical water splitting using nanotubular FeO_x-TiO_2 annealed at different temperatures. *J. Power Sources* **2021**, *507*, 230274.
(14) Hou, S.; Huang, M.-H.; Xiao, F.-X. Stabilizing atomically precise metal nanoclusters as simultaneous charge relay mediators and photosensitizers. *J. Mater. Chem. A* **2022**, *10*, 7006−7012.
(15) Xiao, Y.; Mo, Q. L.; Wu, G.; Wang, K.; Ge, X.-Z.; Xu, S.-R.; Li, J.-L.; Wu, Y.; Xiao, F.-X. Charge modulation over atomically precise metal nanoclusters via non-conjugated polymers for photoelectrochemical water oxidation. *J. Mater. Chem. A* **2023**, *11*, 2402−2411.
(16) Tang, B.; Zhu, S.-C.; Liang, H.; Li, S.; Liu, B.-J.; Xiao, F.-X. Tuning atomically precise metal nanocluster mediated photoelectrocatalysis via a non-conjugated polymer. *J. Mater. Chem. A* **2022**, *10*, 4032−4042.
(17) Stergiopoulos, T.; Ghicov, A.; Likodimos, V.; Tsoukleris, D. S.; Kunze, J.; Schmuki, P.; Falaras, P. Dye-sensitized solar cells based on thick highly ordered TiO_2 nanotubes produced by controlled anodic oxidation in non-aqueous electrolytic media. *Nanotechnology* **2008**, *19*, 235602.
(18) Kim, D.; Roy, P.; Lee, K.; Schmuki, P. Dye-sensitized solar cells using anodic TiO_2 mesosponge: Improved efficiency by $TiCl_4$ treatment. *Electrochem. Commun.* **2010**, *12*, 574−578.
(19) Yang, J. H.; Kim, K. H.; Bark, C. W.; Choi, H. W. The effect of dye-sensitized solar cell based on the composite layer by anodic TiO_2 nanotubes. *Nanoscale Res. Lett.* **2014**, *9*, 671.
(20) Yang, D.-J.; Park, H.; Cho, S.-J.; Kim, H.-G.; Choi, W.-Y. TiO_2-nanotube-based dye-sensitized solar cells fabricated by an efficient anodic oxidation for high surface area. *J. Phys. Chem. Solids* **2008**, *69*, 1272−1275.
(21) Yi, Z.; Zeng, Y.; Wu, H.; Chen, X.; Fan, Y.; Yang, H.; Tang, Y.; Yi, Y.; Wang, J.; Wu, P. Synthesis, surface properties, crystal structure and dye-sensitized solar cell performance of TiO_2 nanotube arrays anodized under different parameters. *Results Phys.* **2019**, *15*, 102609.
(22) Zhang, J. C.; Han, Z. Y.; Li, Q. Y.; Yang, X. Y.; Yu, Y.; Cao, W. L. N, S-doped TiO_2 anode effect on performance of dye-sensitized solar cells. *J. Phys. Chem. Solids* **2011**, *72*, 1239−1244.
(23) Gonzalez-Valls, I.; Mirloup, A.; Le Bahers, T.; Keller, N.; Cottineau, T.; Sautet, P.; Keller, V. Characterization and charge transfer properties of organic BODIPY dyes integrated in TiO_2 nanotube based dye-sensitized solar cells. *RSC Adv.* **2016**, *6*, 91529−91540.
(24) Erten-Ela, S.; Yilmaz, M. D.; Icli, B.; Dede, Y.; Icli, S.; Akkaya, E. U. A Panchromatic Boradiazaindacene (BODIPY) Sensitizer for Dye-Sensitized Solar Cells. *Org. Lett.* **2008**, *10*, 3299−3302.
(25) Wang, L.; Fang, G.; Cao, D. A novel phenol-based BODIPY chemosensor for selective detection Fe^{3+} with colorimetric and fluorometric dual-mode. *Sens. Actuators, B* **2015**, *207*, 849−857.
(26) Ziessel, R.; Ulrich, G.; Haefele, A.; Harriman, A. An Artificial Light-Harvesting Array Constructed from Multiple Bodipy Dyes. *J. Am. Chem. Soc.* **2013**, *135*, 11330−11344.
(27) Liu, J.; He, X.; Zhang, J.; He, T.; Huang, L.; Shen, J.; Li, D.; Qiu, H.; Yin, S. A BODIPY derivative for colorimetric and fluorometric sensing of fluoride ion and its logic gates behavior. *Sens. Actuators, B* **2015**, *208*, 538−545.
(28) Lin, W.; Zhang, W.; Liu, S.; Li, Z.; Hu, X.; Xie, Z.; Duan, C.; Han, G. Engineering pH-Responsive BODIPY Nanoparticles for Tumor Selective Multimodal Imaging and Phototherapy. *ACS Appl. Mater. Interfaces* **2019**, *11*, 43928−43935.
(29) Topa-Skwarczyńska, M.; Świeży, A.; Krok, D.; Starzak, K.; Niezgoda, P.; Oksiuta, B.; Wałczyk, W.; Ortyl, J. Novel Formulations Containing Fluorescent Sensors to Improve the Resolution of 3D Prints. *Int. J. Mol. Sci.* **2022**, *23*, 10470.
(30) Topa-Skwarczyńska, M.; Galek, M.; Jankowska, M.; Morlet-Savary, F.; Graff, B.; Lalevée, J.; Popielarz, R.; Ortyl, J. Development of the first panchromatic BODIPY-based one-component iodonium salts for initiating the photopolymerization processes. *Polym. Chem.* **2021**, *12*, 6873−6893.
(31) Soultati, A.; Nunzi, F.; Fakharuddin, A.; Verykios, A.; Armadorou, K. K.; Tountas, M.; Panagiotakis, S.; Polydorou, E.; Charisiadis, A.; Nikolaou, V.; et al. Functionalized BODIPYs as Tailor-Made and Universal Interlayers for Efficient and Stable Organic and Perovskite Solar Cells. *Adv. Mater. Interfaces* **2022**, *9*, 2102324.
(32) Rousseau, T.; Cravino, A.; Bura, T.; Ulrich, G.; Ziessel, R.; Roncali, J. BODIPY derivatives as donor materials for bulk heterojunction solar cells. *Chem. Commun.* **2009**, 1673−1675.
(33) Dos Santos, J. M.; Jagadamma, L. K.; Cariello, M.; Samuel, D. W.; Cooke, G. A BODIPY small molecule as hole transporting material for efficient perovskite solar cells. *Sustainable Energy Fuels* **2022**, *6*, 4322−4330.
(34) Singh, S. P.; Gayathri, T. Evolution of BODIPY Dyes as Potential Sensitizers for Dye-Sensitized Solar Cells: Sensitizers for Dye-Sensitized Solar Cells. *J. Org. Chem.* **2014**, *2014*, 4689−4707.
(35) Wang, M.; Vicente, M. G. H.; Mason, D.; Bobadova-Parvanova, P. Stability of a Series of BODIPYs in Acidic Conditions: An Experimental and Computational Study into the Role of the Substituents at Boron. *ACS Omega* **2018**, *3*, 5502−5510.
(36) Jayworth, J. A.; Capobianco, M. D.; Liu, H.-Y.; Decavoli, C.; Crabtree, R. H.; Brudvig, G. W. BODIPY and dipyrrin as unexpected robust anchoring groups on TiO_2 nanoparticles. *Dalton Trans.* **2022**, *51*, 14260−14266.
(37) Jarosz, M.; Kapusta-Kołodziej, J.; Jaskuła, M.; Sulka, G. D. Effect of different polishing methods on anodic titanium dioxide formation. *J. Nanomater.* **2015**, *2015*, 1−10.
(38) Lu, Q.; Zhu, L.; Han, S.; Hou, Y.; Cao, W. Photocatalytic synthesis of gold nanoparticles using TiO_2 nanorods: a mechanistic investigation. *Phys. Chem. Chem. Phys.* **2019**, *21*, 18753−18757.

https://doi.org/10.1021/acs.jpcc.3c00931
J. Phys. Chem. C 2023, 127, 9471−9480

(39) Reichardt, C. Solvatochromic dyes as solvent polarity indicators. *Chem. Rev.* **1994**, *94*, 2319−2358.
(40) Topa, M.; Petko, F.; Galek, M.; Jankowska, M.; Popielarz, R.; Ortyl, J. Difunctional 1H-quinolin-2-ones as spectroscopic fluorescent probes for real-time monitoring of photopolymerisation process and photosensitizers of fluorescent photopolymer resin in 3D printing. *Eur. Polym. J.* **2021**, *156*, 110612.
(41) Wang, K.; Liu, G.; Hoivik, N.; Johannessen, E.; Jakobsen, H. Electrochemical engineering of hollow nanoarchitectures: pulse/step anodization (Si, Al, Ti) and their applications. *Chem. Soc. Rev.* **2014**, *43*, 1476−1500.
(42) Brudzisz, A.; Brzózka, A.; Sulka, G. D. Effect of processing parameters on pore opening and mechanism of voltage pulse detachment of nanoporous anodic alumina. *Electrochim. Acta* **2015**, *178*, 374−384.
(43) Sulka, G. D.; Kapusta-Kołodziej, J.; Brzózka, A.; Jaskuła, M. Fabrication of nanoporous TiO_2 by electrochemical anodization. *Electrochim. Acta* **2010**, *55*, 4359−4367.
(44) Gong, J.; Lai, Y.; Lin, C. Electrochemically multi-anodized TiO_2 nanotube arrays for enhancing hydrogen generation by photoelectrocatalytic water splitting. *Electrochim. Acta* **2010**, *55*, 4776−4782.
(45) Acevedo-Peña, P.; Carrera-Crespo, J. E.; González, F.; González, I. Effect of Heat Treatment on the Crystal Phase Composition, Semiconducting Properties and Photoelectrocatalytic Color Removal Efficiency of TiO_2 Nanotubes Arrays. *Electrochim. Acta* **2014**, *140*, 564−571.
(46) Park, J.-W.; Shumaker-Parry, J. S. Structural Study of Citrate Layers on Gold Nanoparticles: Role of Intermolecular Interactions in Stabilizing Nanoparticles. *J. Am. Chem. Soc.* **2014**, *136*, 1907−1921.
(47) Ambroz, F.; Donnelly, J. L.; Wilden, J. D.; Macdonald, T. J.; Parkin, I. P. Carboxylic Acid Functionalization at the Meso-Position of the Bodipy Core and Its Influence on Photovoltaic Performance. *Nanomaterials* **2019**, *9*, 1346.
(48) Gee, W. J.; Shepherd, H. J.; Dawson, D. M.; Ashbrook, S. E.; Raithby, P. R.; Burrows, A. D. Solid-state host−guest influences on a BODIPY dye hosted within a crystalline sponge. *New J. Chem.* **2020**, *44*, 14108−14115.
(49) Pisarek, M.; Krawczyk, M.; Kosiński, A.; Hołdyński, M.; Andrzejczuk, M.; Krajczewski, J.; Bieńkowski, K.; Solarska, R.; Gurgul, M.; Zaraska, L.; et al. Materials characterization of TiO_2 nanotubes decorated by Au nanoparticles for photoelectrochemical applications. *RSC Adv.* **2021**, *11*, 38727−38738.
(50) Naldoni, A.; Riboni, F.; Marelli, M.; Bossola, F.; Ulisse, G.; Di Carlo, A.; Píš, I.; Nappini, S.; Malvestuto, M.; Dozzi, M. V.; et al. Influence of TiO_2 electronic structure and strong metal−support interaction on plasmonic Au photocatalytic oxidations. *Catal. Sci. Technol.* **2016**, *6*, 3220−3229.
(51) Tang, H.; Wei, J.; Liu, F.; Qiao, B.; Pan, X.; Li, L.; Liu, J.; Wang, J.; Zhang, T. Strong Metal−Support Interactions between Gold Nanoparticles and Nonoxides. *J. Am. Chem. Soc.* **2016**, *138*, 56−59.
(52) Chen, H.; Yang, Z.; Wang, X.; Polo-Garzon, F.; Halstenberg, P. W.; Wang, T.; Suo, X.; Yang, S.-Z.; Meyer, H. M.; Wu, Z.; et al. Photoinduced Strong Metal−Support Interaction for Enhanced Catalysis. *J. Am. Chem. Soc.* **2021**, *143*, 8521−8526.
(53) Xu, Y.; Wu, S.; Wan, P.; Sun, J.; Hood, Z. D. Introducing Ti^{3+} defects based on lattice distortion for enhanced visible light photoreactivity in TiO_2 microspheres. *RSC Adv.* **2017**, *7*, 32461−32467.
(54) Kumaresan, D.; Thummel, R. P.; Bura, T.; Ulrich, G.; Ziessel, R. Color Tuning in New Metal-Free Organic Sensitizers (Bodipys) for Dye-Sensitized Solar Cells. *Chem.—Eur. J.* **2009**, *15*, 6335−6339.
(55) Luna, M.; Barawi, M.; Gómez-Moñivas, S.; Colchero, J.; Rodríguez-Peña, M.; Yang, S.; Zhao, X.; Lu, Y.-H.; Chintala, R.; Reñones, P.; et al. Photoinduced Charge Transfer and Trapping on Single Gold Metal Nanoparticles on TiO_2. *ACS Appl. Mater. Interfaces* **2021**, *13*, 50531−50538.
(56) Schmidt-Mende, L.; Campbell, W. M.; Wang, Q.; Jolley, K. W.; Officer, D. L.; Nazeeruddin, M. K.; Grätzel, M. Zn-Porphyrin-Sensitized Nanocrystalline TiO_2 Heterojunction Photovoltaic Cells. *ChemPhysChem* **2005**, *6*, 1253−1258.
(57) Basumatary, P.; Agarwal, P. Photocurrent transient measurements in $MAPbI_3$ thin films. *J. Mater. Sci.: Mater. Electron.* **2020**, *31*, 10047−10054.
(58) Radecka, M.; Wierzbicka, M.; Komornicki, S.; Rekas, M. Influence of Cr on photoelectrochemical properties of TiO_2 thin films. *Phys. B* **2004**, *348*, 160−168.
(59) Syrek, K.; Skolarczyk, M.; Zych, M.; Sołtys-Mróz, M.; Sulka, G. D. A Photoelectrochemical Sensor Based on Anodic TiO_2 for Glucose Determination. *Sensors* **2019**, *19*, 4981.
(60) Denisov, N.; Yoo, J. E.; Schmuki, P. Effect of different hole scavengers on the photoelectrochemical properties and photocatalytic hydrogen evolution performance of pristine and Pt-decorated TiO_2 nanotubes. *Electrochim. Acta* **2019**, *319*, 61−71.
(61) Liu, J.; Fan, C.; Xie, X.; Jiang, L. Recent Progress on Photo-Promoted Alcohol Electrooxidation for Fuel Cells. *Energy Technol.* **2021**, *9*, 2000842.
(62) Nakajima, T.; Hagino, A.; Nakamura, T.; Tsuchiya, T.; Sayama, K. WO_3 nanosponge photoanodes with high applied bias photon-to-current efficiency for solar hydrogen and peroxydisulfate production. *J. Mater. Chem. A* **2016**, *4*, 17809−17818.
(63) Wierzbicka, E.; Schultz, T.; Syrek, K.; Sulka, G. D.; Koch, N.; Pinna, N. Ultra-stable self-standing Au nanowires/TiO_2 nanoporous membrane system for high-performance photoelectrochemical water splitting cells. *Mater. Horiz.* **2022**, *9*, 2797−2808.
(64) Solaiyammal, T.; Murugakoothan, P. Green synthesis of Au and the impact of Au on the efficiency of TiO_2 based dye sensitized solar cell. *Mater. Sci. Energy Technol.* **2019**, *2*, 171−180.
(65) Du, J.; Qi, J.; Wang, D.; Tang, Z. Facile synthesis of Au@TiO_2 core-shell hollow spheres for dye-sensitized solar cells with remarkably improved efficiency. *Energy Environ. Sci.* **2012**, *5*, 6914−6918.

https://doi.org/10.1021/acs.jpcc.3c00931
J. Phys. Chem. C 2023, 127, 9471−9480